Signal Estimation from Incomplete Data on the Sphere

Wen Zhang, Rodney A. Kennedy and Thushara D. Abhayapala
Department of Information Engineering
Research School of Information Sciences and Engineering
The Australian National University
Email: wen@cecs.anu.edu.au, rodney.kennedy@anu.edu.au, thushara.abhayapala@anu.edu.au

***Abstract*—An iterative algorithm is proposed to estimate a signal on the sphere from limited or incomplete measurements. The algorithm is based on a priori assumption that the Fourier decomposition of the signal on the sphere has finite degree of spherical harmonic coefficients, that is, the signal is *mode-limited* or low-pass in character. The iteration algorithm is to reduce the mean square error between the spherical harmonic coefficients of the estimated and that of the original signal. Convergence and its numerical properties are determined using spherical harmonic analysis. A practical example of antenna radiation pattern reconstruction is given with detailed analysis.**

***Index Terms*—Signal Estimation, Incomplete data, Sphere, Spherical Harmonics, Modelimited**

I. Introduction

The problem of finding an estimate of a signal outside an observation interval plays a central role in many signal processing applications. Several algorithms have been proposed for bandlimited signal extrapolation from measurements on a finite time interval [1], [2], [3]. Some of them have also been used in image signal processing [4] due to the natural extension of the Fourier Transform to the 2-D case. In this paper, we address the problem of estimating discrete modelimited signals on the sphere from an incomplete set of measurements. Such estimation problem is of great practical significance to experimental data reconstruction over the whole sphere from limited or incomplete measurements, such as the spherical radiation pattern of antenna systems. The measurements at low elevation angles can be absent due to the limit caused by the measuring apparatus. In other situations data corruption necessitates that in order to obtain the correct pattern, these corrupted measurements should be removed and the algorithm proposed in this paper gives an efficient method to accurately estimate antenna radiation pattern from the remaining limited data.

Let S^2 denote the unit sphere in three dimensions. The *Estimation Problem* in this paper is to find the original signal $f(\theta,\phi)$ over the whole sphere from the incomplete measurements $g(\theta,\phi)$ given over an observation region Γ ($\Gamma \subset S^2$, $(\theta,\phi) \in \Gamma$). It is well known that the spherical harmonics, $Y_n^m(\theta,\phi)$, for $m=-n,\cdots,n$, $n=0,1,2,\cdots$, form a complete orthogonal basis in $L^2(S^2)$ with the natural inner product [5], [10]. Here, the angle $0^\circ \le \theta \le 180^\circ$ is the polar angle, or colatitude and $0^\circ \le \phi \le 360^\circ$ is the azimuthal angle. The expansion of a function $f \in L^2(S^2)$ can be written as

$$f(\theta,\phi)=\sum_{n=0}^{\infty}\sum_{m=-n}^{n} F_{nm}Y_n^m(\theta,\phi). \tag{1}$$

F_{nm} are the spherical harmonic coefficients of degree n and order m obtained by projecting f onto Y_n^m, i.e.,

$$F_{nm}=\int_{S^2} f(\theta,\phi)Y_n^m(\theta,\phi)^* d\Omega, \tag{2}$$

where Ω is the solid angle with integral defined by $\int_{S^2} d\Omega \equiv \int_0^{2\pi} d\phi \int_0^{\pi} \sin\theta d\theta$, and the $(\cdot)^*$ stands for complex conjugate.

To find the original signal $f(\theta,\phi)$, a prior assumption is that the function is *mode-limited*, that is, its energy is finite and its spherical harmonic coefficients F_{nm} are zero above a certain degree N, i.e.,

$$F_{nm}=0, \text{ for } |n| \ge N. \tag{3}$$

The assumption is made based on two reasons: i) analogous to bandlimited property of temporal signals, we expect the original signal $f(\theta,\phi)$ to be smooth and can be represented with a finite number of spherical harmonics; ii) in practice the integral to solve spherical harmonic coefficients as in (2) is approximated from a set of discrete experimental measurements using specific sampling arrangements [6], [7]. This approximation can only unambiguously determine a finite number of spherical harmonic coefficients, say for degrees $0 \le n < N$. Knowing F_{nm} is equivalent to knowing $f(\theta,\phi)$. Further under (3), we need only a finite number of F_{nm} coefficients so we can understand the modelimited function on the sphere as a finite dimensional vector space (of dimension N^2).

The proposed extrapolation algorithm is an iterative algorithm (related to the Papoulis algorithm [3] for bandlimited extrapolation) based on the spherical harmonic decomposition of the signal over the sphere. The problem is to recover the modelimited spherical harmonic coefficients of the original data from the incomplete measurements. It is shown that the Euclidean norm between the spherical harmonic coefficients of the estimated and that of the original signal reduces at successive iterations. Using this error energy reduction procedure, we will show that the estimates converge to the original signal (strong convergence in the norm). In addition,

the convergence is bounded by the minimum eigenvalue of a Hermitian operator, which is a function only of the observation region. Finally, the estimation of antenna radiation pattern with corrupted data is given as a practical example.

II. Iterative Algorithm

The proposed method is based on an iterative algorithm involving only the spherical harmonic expansion of functions on the sphere. To determine the modelimited function $f(\theta,\phi)$ from limited measurements $g(\theta,\phi)$ over the observation region Γ, the iterative algorithm starts from computing spherical harmonic coefficients

$$F_{nm}^{(1)} = \begin{cases} \int_\Gamma g(\theta,\phi) Y_n^m(\theta,\phi)^* d\Omega & |n| < N \\ 0 & |n| \geq N \end{cases} \tag{4}$$

where $d\Omega = \sin\theta d\theta d\phi$. In practice, as stated integral (4) is performed by summation; and from (4) we can compute a modelimited function

$$f_1(\theta,\phi) = \sum_{n=0}^{N-1} \sum_{m=-n}^{n} F_{nm}^{(1)} Y_n^m(\theta,\phi). \tag{5}$$

Next, we replace the segment of $f_1(\theta,\phi)$ over the observation region Γ by the known data $g(\theta,\phi)$

$$g_1(\theta,\phi) = \begin{cases} g(\theta,\phi) & (\theta,\phi) \in \Gamma \\ f_1(\theta,\phi) & \text{elsewhere.} \end{cases} \tag{6}$$

Following the same procedure, at the k^{th} iteration, we have

$$F_{nm}^{(k)} = \begin{cases} \int_{S^2} g_{k-1}(\theta,\phi) Y_n^m(\theta,\phi)^* d\Omega & |n| < N \\ 0 & |n| \geq N \end{cases} \tag{7}$$

and

$$f_k(\theta,\phi) = \sum_{n=0}^{N-1} \sum_{m=-n}^{n} F_{nm}^{(k)} Y_n^m(\theta,\phi). \tag{8}$$

Thus,

$$\begin{aligned} g_k(\theta,\phi) &= \begin{cases} g(\theta,\phi) & (\theta,\phi) \in \Gamma \\ f_k(\theta,\phi) & \text{elsewhere} \end{cases} \\ &= f_k(\theta,\phi) + \big(D_\Gamma[f - f_k]\big)(\theta,\phi), \end{aligned} \tag{9}$$

where D_Γ is defined as a space selecting operator

$$\big(D_\Gamma f\big)(\theta,\phi) = \begin{cases} f(\theta,\phi) & (\theta,\phi) \in \Gamma \\ 0 & \text{elsewhere.} \end{cases} \tag{10}$$

Note that in the algorithm, the computed function $f_k(\theta,\phi)$ after each iteration is modelimited. Thus, we could form that

$$F_{nm}^{(k)} = \beta_n^N G_{nm}^{(k-1)}, \tag{11}$$

where $G_{nm}^{(k-1)}$ are the spherical harmonic coefficients of $g_{k-1}(\theta,\phi)$ defined for $n \in [0,\infty)$, and β_n^N is defined as

$$\beta_n^N = \begin{cases} 1 & |n| < N \\ 0 & |n| \geq N \end{cases} \tag{12}$$

and corresponds to a modelimited operator B_N on the sphere. That is,

$$f_k(\theta,\phi) = \big(B_N g_{k-1}\big)(\theta,\phi). \tag{13}$$

The operator B_N can be regarded as a low-pass spatial filtering operator, it truncates the spherical harmonics of a function to a certain degree N.

Therefore, this algorithm states that we start by low-pass filtering the zero extended observations. At step k, the low-pass filter output $f_k(\theta,\phi)$ is substituted by the observations $g(\theta,\phi)$ over the region Γ and the result is low-pass filtered again to yield $f_{k+1}(\theta,\phi)$. It will be shown in the next section that $f(\theta,\phi)$ and $f_k(\theta,\phi)$ are in the same modelimited subspace. And it will be proven that $f_k(\theta,\phi)$ tends to $f(\theta,\phi)$ as $k \to \infty$, and the convergence properties will be determined.

Numerical Example

We apply the proposed method to extrapolate an incomplete data on a sphere. The data is artificially generated using functional spherical harmonic expansion given in (1) by assigning specific spherical harmonic coefficients but limited in degree $|n| < N$. In the example, the signal is assumed to be mode limited to $N = 4$ and random values are assigned to the spherical harmonic coefficients. The observations are given for $0 \leq \theta \leq 140°$, $0 \leq \phi \leq 300°$. Fig. 1 shows the original signal, the given observations and the estimated signal after 30 iterations. It appears that the iterative algorithm provides an efficient way to estimate signal outside the observation region.

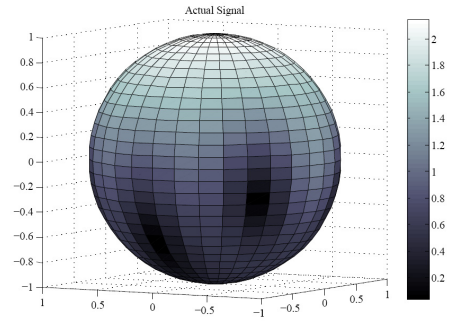

(a) Original signal $f(\theta,\phi)$.

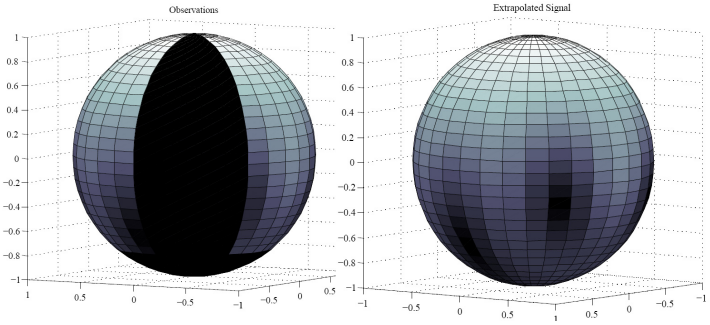

(b) Given Observations $g(\theta,\phi)$ (c) Extrapolated signal $f_k(\theta,\phi)$

Fig. 1. An example of data reconstruction on the sphere using the proposed iterative algorithm. The observations in (b) are given for $0 \leq \theta \leq 140°$, $0 \leq \phi \leq 300°$ with $N = 4$. Extrapolation results in (c) are the estimates after 30 iterations. The color scale shows the signal magnitude; and the pure black means no observation made.

III. Illustration of the Algorithm

Given the modelimited property of $f(\theta,\phi)$, we have

$$f(\theta,\phi) = \big(B_N f\big)(\theta,\phi), \tag{14}$$

and the space selected function is given by

$$g(\theta,\phi) = \big(D_\Gamma f\big)(\theta,\phi). \tag{15}$$

The collection of modelimited functions forms a complete linear subspace $\mathcal{B}$ (modelimited subspace) of $L^2(S^2)$ so that all functions having the same finite degree spherical harmonic coefficients are in the same subspace. Analogously, the space selected functions form another complete linear subspace $\mathcal{D}$ (space selection subspace) of $L^2(S^2)$. Then, as shown in Fig. 2, the iterative algorithm can be regarded as an affine projection involving D_Γ, given in (10) and an orthogonal projection using B_N given in (13). Thus we have

$$\begin{aligned} f_k(\theta,\phi) &= \big(B_N g_{k-1}\big)(\theta,\phi) \\ &= \big(B_N f_{k-1}\big)(\theta,\phi) + \big(B_N D_\Gamma[f - f_{k-1}]\big)(\theta,\phi) \\ &= f_{k-1}(\theta,\phi) + \big(B_N g\big)(\theta,\phi) - \big(B_N D_\Gamma f_{k-1}\big)(\theta,\phi). \end{aligned} \tag{16}$$

Here $f_k(\theta,\phi) = \big(B_N f_k\big)(\theta,\phi)$ because f_k is in the modelimited subspace. The algorithm can be interpreted as an iterative descent algorithm. Here by descent, we mean that in the modelimited subspace, each new point f_k generated by the algorithm corresponds to reducing the value of some error function $(f - f_k)$. Intuitively, the sequence of points generated by such algorithm converges to the original signal. In the next section, we will use spherical harmonic analysis to prove the convergence of the algorithm.

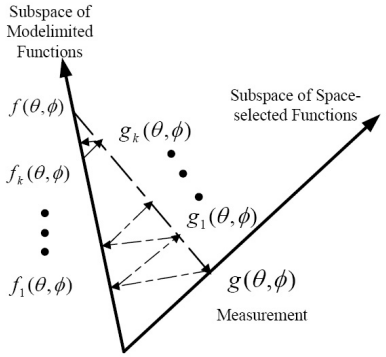

Fig. 2. Illustration of the algorithm as projections involving two subspaces, the modelimited subspace and the space selection subspace, corresponding to the modelimited signal and given measurements.

IV. Convergence

The representation of a signal with the spherical harmonics using (2) is in essence the orthogonal decomposition of the signal in the Hilbert space $L^2(S^2)$. On the sphere, there is a *one-to-one correspondence* between the signal $f(\theta,\phi)$ and its spherical harmonic coefficients F_{nm}. Thus equivalently, to prove the convergence of the algorithm, we examine the approximation error between $F_{nm}^{(k+1)}$ and F_{nm} after each iteration.

Theorem 1. *At the $k+1^{th}$ iteration of the algorithm,*

$$\boldsymbol{F}^{(k+1)} = \boldsymbol{F}^{(k)} + \boldsymbol{G} - \boldsymbol{M}_\Gamma \boldsymbol{F}^{(k)}, \tag{17}$$

where $\boldsymbol{F}^{(k+1)}$, $\boldsymbol{F}^{(k)}$ and $\boldsymbol{G}$ are spherical harmonic coefficients of signal $f_{k+1}(\theta,\phi)$, $f_k(\theta,\phi)$ and $g(\theta,\phi)$ in the vector form but modelimited to degree N. $\boldsymbol{M}_\Gamma$ is a matrix operator for mode scrambling and determined by the observation region Γ.

Proof: From (16) and

$$F_{nm}^{(k+1)} = \int_{S^2} f_{k+1}(\theta,\phi) Y_n^m(\theta,\phi)^* d\Omega, \tag{18}$$

we can obtain

$$F_{nm}^{(k+1)} = F_{nm}^{(k)} + G_{nm} - \int_\Gamma f_k(\theta,\phi) Y_n^m(\theta,\phi)^* d\Omega \tag{19}$$

for $0 \le n < N$ (remember f_k is a modelimited function with the spherical harmonic coefficients up to degree N, here G_{nm} and $\int_\Gamma f_k(\theta,\phi) Y_n^m(\theta,\phi)^* d\Omega$ are also truncated to the same degree). Replacing the spherical harmonic decomposition of $f_k(\theta,\phi)$ as shown in (8) into (19), we get

$$\begin{aligned} F_{nm}^{(k+1)} = F_{nm}^{(k)} + G_{nm} - \\ \int_\Gamma \sum_{p=0}^{N-1} \sum_{q=-p}^{p} F_{pq}^{(k)} Y_p^q(\theta,\phi) Y_n^m(\theta,\phi)^* d\Omega. \end{aligned} \tag{20}$$

Thus the generalized vector form can be written as

$$\mathbf{F}^{(k+1)} = \mathbf{F}^{(k)} + \mathbf{G} - \mathbf{M}_\Gamma \mathbf{F}^{(k)}, \tag{21}$$

where the spherical harmonic coefficients $\mathbf{F}^{(k+1)}$, $\mathbf{G}$ are arranged as $N^2 * 1$ column vectors

$$\mathbf{F}^{(k+1)} = (\alpha_1^{(k+1)} \ \cdots \ \alpha_i^{(k+1)} \ \cdots \ \alpha_{N^2}^{(k+1)})^T \tag{22}$$

$$\mathbf{G} = (\beta_1 \ \cdots \ \beta_i \ \cdots \ \beta_{N^2})^T \tag{23}$$

by assigning $\alpha_i^{(k+1)} = F_{nm}^{(k+1)}$ and $\beta_i = G_{nm}$ with $i = n(n+1) + (m+1)$ for $n = 0, 1, \cdots, N-1$ and $m = -n, \cdots, n$. $\mathbf{M}_\Gamma$ is a $N^2 * N^2$ matrix operator

$$\mathbf{M}_\Gamma = \begin{pmatrix} \gamma_{11} & \cdots & \gamma_{1j} & \cdots & \gamma_{1N^2} \\ \vdots & \ddots & \vdots & \vdots & \vdots \\ \gamma_{i1} & \cdots & \gamma_{ij} & \cdots & \gamma_{iN^2} \\ \vdots & \vdots & \vdots & \ddots & \vdots \\ \gamma_{N^21} & \cdots & \gamma_{N^2j} & \cdots & \gamma_{N^2N^2} \end{pmatrix}, \tag{24}$$

where

$$\gamma_{ij} = \int_\Gamma Y_p^q(\theta,\phi) Y_n^m(\theta,\phi)^* d\Omega \tag{25}$$

with assignment of $i = n(n+1) + (m+1)$ and $j = p(p+1) + (q+1)$. ■

As spherical harmonics indexes n, p are both truncated to degree N and m, q also vary in the same range between $-n, \ldots, n$ (or $-p, \ldots, p$), it can be observed that $\gamma_{ij} = \gamma_{ji}^*$. Thus, the matrix operator $\mathbf{M}_\Gamma$ is Hermitian and positive

definite. When performing an eigen-decomposition, it has a set of real positive eigenvalues λ_i and orthogonal eigenvectors φ_i, that is,

$$\mathbf{M}_\Gamma U = U\Lambda, \tag{26}$$

where U is formed by the columns of the orthogonal eigenvectors

$$U = \begin{pmatrix} \varphi_0 & \varphi_1 & \cdots & \varphi_{N^2} \end{pmatrix}. \tag{27}$$

Both U and U^{-1} are unitary matrixes. And Λ is a diagonal matrix with entries being the eigenvalues

$$\Lambda = \begin{pmatrix} \lambda_0 & 0 & \cdots & 0 \\ 0 & \lambda_1 & \cdots & 0 \\ \vdots & \vdots & \ddots & \vdots \\ 0 & 0 & \cdots & \lambda_{N^2} \end{pmatrix} \tag{28}$$

Note $0 < \lambda_i \leq 1$, and only when $\Gamma = S^2$, $\mathbf{M}_\Gamma$ is an identity matrix and has all eigenvalues equal to 1.

Theorem 2. *$\boldsymbol{F}^{(k)}$ converges to the original modelimited spherical harmonic coefficients $\boldsymbol{F}$, that is,*

$$\boldsymbol{F}^{(k)} \to \boldsymbol{F}, \text{ as } k \to \infty. \tag{29}$$

Proof: Referring to Theorem 1, $\mathbf{G}$ and $\mathbf{M}_\Gamma$ are fixed functions of measurements and observation region, respectively. From (15) we have

$$\begin{aligned} \mathbf{G} &= \int_\Gamma f(\theta,\phi) Y_n^m(\theta,\phi)^* d\Omega \\ &= \mathbf{M}_\Gamma \mathbf{F}. \end{aligned} \tag{30}$$

Then after each iteration

$$\begin{aligned} (\mathbf{F}^{(k+1)} - \mathbf{F}) &= (\mathbf{I} - \mathbf{M}_\Gamma)(\mathbf{F}^{(k)} - \mathbf{F}) + \mathbf{G} - \mathbf{M}_\Gamma \mathbf{F} \\ &= (\mathbf{I} - \mathbf{M}_\Gamma)(\mathbf{F}^{(k)} - \mathbf{F}), \end{aligned} \tag{31}$$

where $\mathbf{I}$ is the identity matrix. Given (26), we have

$$(\mathbf{I} - \mathbf{M}_\Gamma) = U(\mathbf{I} - \Lambda)U^{-1}. \tag{32}$$

If we define the estimation error as the Euclidean norm of $(\mathbf{F}^{(k+1)} - \mathbf{F})$

$$\begin{aligned} e^{(k+1)} &= \|\mathbf{F}^{(k+1)} - \mathbf{F}\|_2 \\ &= \|\mathbf{I} - \mathbf{M}_\Gamma\|_2 \|\mathbf{F}^{(k)} - \mathbf{F}\|_2 \\ &= \|U(\mathbf{I} - \Lambda)U^{-1}\|_2 \|\mathbf{F}^{(k)} - \mathbf{F}\|_2 \\ &= \|(\mathbf{I} - \Lambda)\|_2 \|\mathbf{F}^{(k)} - \mathbf{F}\|_2 \end{aligned} \tag{33}$$

where $\|(\mathbf{I} - \Lambda)\|_2$ is the spectral norm, the induced matrix norm from the vector Euclidean norm. As the spectral norm of a matrix is defined as the largest singular value of the matrix, (33) reduces to

$$e^{(k+1)} = (1 - \lambda_{\min})\|\mathbf{F}^{(k)} - \mathbf{F}\|_2, \tag{34}$$

where $\lambda_{\min}$ is the smallest eigenvalue of $\mathbf{M}_\Gamma$.

As stated, $0 < \lambda_{\min} \leq 1$, we have $0 \leq (1 - \lambda_{\min}) < 1$; and it can be seen that

$$\frac{e^{(k+1)}}{e^{(k)}} = \frac{\|\mathbf{F}^{(k+1)} - \mathbf{F}\|_2}{\|\mathbf{F}^{(k)} - \mathbf{F}\|_2} = 1 - \lambda_{\min} < 1. \tag{35}$$

This shows that the estimation error reduces at successive iterations, or the convergence of $\mathbf{F}^{(k)}$ to the original modelimited spherical harmonic coefficients $\mathbf{F}$, that is,

$$\|\mathbf{F}^{(k)} - \mathbf{F}\|_2 \to 0, \text{ as } k \to \infty. \tag{36}$$

■

Corollary 3. *The estimates f_k converge in the mean to the original function f over the sphere, i.e.,*

$$f_k(\theta,\phi) \to f(\theta,\phi), \text{ as } k \to \infty. \tag{37}$$

Proof: From the generalized Parseval's theorem [8], we have

$$\|f(\theta,\phi)\|_2 \triangleq \int_{S^2} \|f(\theta,\phi)\|^2 d\Omega = \|\mathbf{F}\|_2. \tag{38}$$

From (36), this implies

$$\|f_k(\theta,\phi) - f(\theta,\phi)\|_2 \to 0, \text{ as } k \to \infty, \tag{39}$$

thus $f_k(\theta,\phi)$ converges to the $f(\theta,\phi)$ in the mean. In summary, the algorithm provides a strong convergence. ■

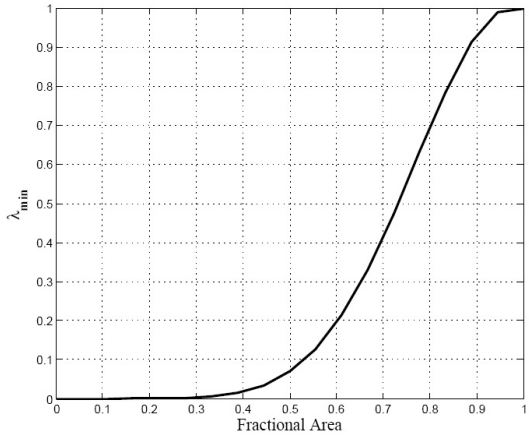

Fig. 3. An example of $\lambda_{\min}$ increasing with the area of observation region, where the colatitude observations increase from 0° to 180° and the full range of azimuthal observation is assumed. The observation region is represented by fractional area ($\int_\Gamma d\Omega/4\pi$), the solid angles in fractions of the sphere.

As stated $\mathbf{M}_\Gamma$ is a function of the observation region Γ. And Fig. 3 shows that $\lambda_{\min}$, the smallest eigenvalue of $\mathbf{M}_\Gamma$, increases with the observation area Γ. In addition, as shown in (34), the estimation error of the iteration algorithm is inversely related to the smallest eigenvalue $\lambda_{\min}$. It means that measurements of larger observation regions have faster convergence and thus would tend to require a smaller number of iterations.

Fig. 4 numerically demonstrates the algorithm's convergence performance, giving the mean-square estimation error between the estimated and original signal after each iteration for different observation regions. Several observations are: Firstly, the estimation error is exponentially decaying with the iteration step, demonstrating that the convergence of $\mathbf{F}^k$ to the unknown modelimited spherical harmonic coefficients

F is rapid. Secondly, there are generally a smaller error and faster convergence associated with the measurements of larger observation regions.

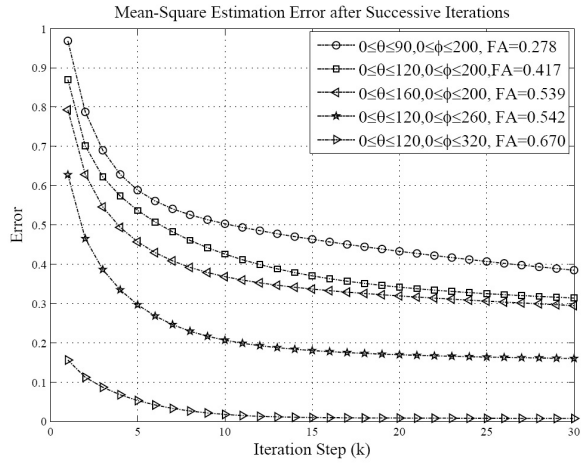

Fig. 4. Mean square error between the estimated and original signal for different data observation regions. FA stands for fractional area and the spherical harmonic coefficients are resolved to degree $N = 4$.

V. Practical Example: Antenna Radiation Pattern

Being the solutions to the Helmholtz wave equations and describing the propagation properties of the electromagnetic waves, spherical harmonics form a natural orthogonal basis for the expansion of antenna radiation pattern [9], [10]

$$E(r,\theta,\phi) = \sum_{n=0}^{\infty}\sum_{m=-n}^{n} A_{nm} h_n^{(1)}(\eta r) Y_n^m(\theta,\phi), \qquad (40)$$

where $E(\cdot)$ is the electrical field strength, $h_n^{(1)}(\eta r)$ is the spherical Hankel function, representing the range dependence. $\eta = 2\pi/\lambda$ is the free-space wave number and λ is the wavelength. In the far-field, the dependence of the radiation pattern on the range variable r is negligible; thus only the spherical harmonics with dependence on the spatial variables θ and ϕ will be of interest. Equation (40) can reduce to

$$E(\theta,\phi) = \sum_{n=0}^{\infty}\sum_{m=-n}^{n} C_{nm} Y_n^m(\theta,\phi). \qquad (41)$$

The above theory provides solutions to solve the problem of estimating antenna radiation pattern using the proposed iterative algorithm.

In this section, the signal estimation procedure described previously in section II is applied to the example of a linear dipole radiation pattern reconstruction. In the spherical coordinate system, the radiation pattern for the z-oriented dipole is omni-directional with respect to the azimuthal angle ϕ and can be represented in the analytical form as [11]

$$E(\theta) = \frac{j60[I_0]}{r_0}\left\{\frac{\cos[(\eta L\cos\theta)/2] - \cos(\eta L/2)}{\sin\theta}\right\}, \qquad (42)$$

where $[I_0] = I_0 \exp\{-jw(t - r_0/c)\}$ is the retarded current with $j = \sqrt{-1}$ and the angular frequency $w = 2\pi f = 2\pi c/\lambda$. c is the speed of light in vacuum, r_0 is the distance from the dipole to the point where the electrical field E is evaluated and L is the length of antenna.

Especially for a $\lambda/2$ dipole the pattern reduces to

$$E(\theta) = \frac{j60[I_0]}{r_0}\left\{\frac{\cos[(\pi\cos\theta)/2]}{\sin\theta}\right\}, \qquad (43)$$

and for a $3\lambda/2$ the pattern is

$$E(\theta) = \frac{j60[I_0]}{r_0}\left\{\frac{\cos[(3\pi\cos\theta)/2]}{\sin\theta}\right\}. \qquad (44)$$

Two examples are performed: the first one is to estimate signal with incomplete observations. Fig.s 5 and 6 show the radiation pattern plots for above two kinds of dipole antennas, with the incomplete measurements denoted by the triangles, the estimation pattern after 50 iterations indicated by the solid curve and the analytical pattern given by the dashed line. In the example, we assign the value $I_0 = 0.5$A, $\lambda = 1$m and $r_0 = 25$m; the observations are given for $0 \le \theta \le 140°$ and $0 \le \phi \le 360°$ and the spherical harmonic coefficients are solved up to degree $N = 8$. The very accurate reconstruction to the data given over the observation region can be observed. While there are gaps between the estimated pattern and the analytical pattern over the data missing region, it is mainly caused by the model truncation error. That is the synthetic data may contain high-order modal terms so that extraneous side-lobes are generated. To get the best estimation, according to [3], the algorithm requires the model truncation number as close as possible to the original signal bandwidth. But given the very accurate reconstruction results over the observation region, we believe the proposed iterative method is an efficient algorithm in practice to estimate unknown antenna pattern from limited measurements.

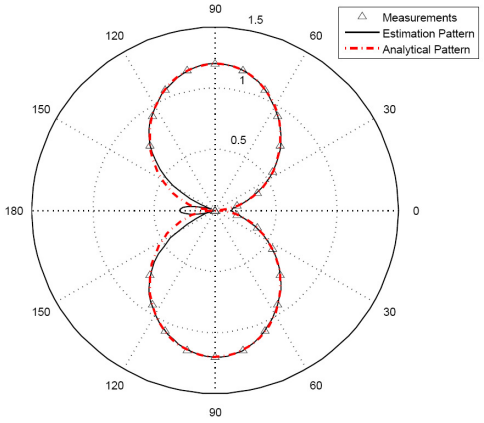

Fig. 5. Radiation pattern estimation for a $\lambda/2$ dipole with spherical harmonic decomposition up to $N = 8$. The observations are given for $0 \le \theta \le 140°$ and $0 \le \phi \le 360°$.

The second case is a more practical example to extrapolate observations containing additive white noise with zero mean and variance $\sigma_0^2 = 0.2$. Fig. 7 and Fig. 8 give two more radiation pattern estimation results. The relative larger errors

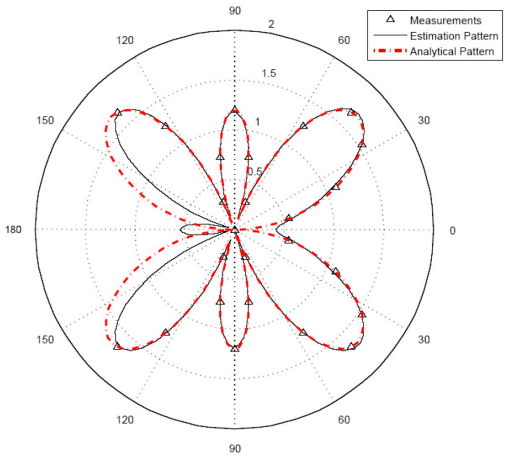

Fig. 6. Radiation pattern estimation for a $3\lambda/2$ dipole with spherical harmonic decomposition up to $N = 8$. The observations are given for $0 \leq \theta \leq 140°$ and $0 \leq \phi \leq 360°$.

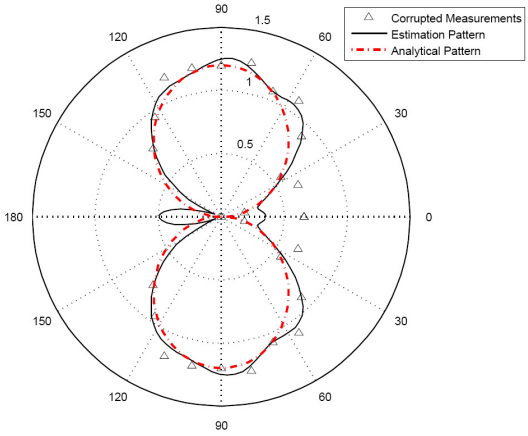

Fig. 7. Radiation pattern estimation for a $\lambda/2$ dipole with corrupted data with spherical harmonic decomposition up to $N = 8$. The observations are given for $0 \leq \theta \leq 140°$ and $0 \leq \phi \leq 360°$.

compared to the previous examples are caused by the corrupted measurements. But we can observe that the estimation pattern can still follow the trend of the analytical pattern.

Throughout these two kinds of dipoles, it can be seen that the radiation pattern goes from having a single main lobe to a main lobe with distinct side lobes. Even though the radiation pattern becomes more complicated, the spherical harmonic expansion can follow the changes with a high degree of accuracy, which indicates that the spherical harmonics are capable of representing the antenna radiation pattern efficiently. Therefore, another advantage associated with using the proposed estimation method is that it provides a continuous representation of the signal in the spatial domain based on the spherical harmonic expansion of the signal.

VI. Conclusion

This paper has presented an iterative algorithm for signal estimation over the sphere from limited or incomplete

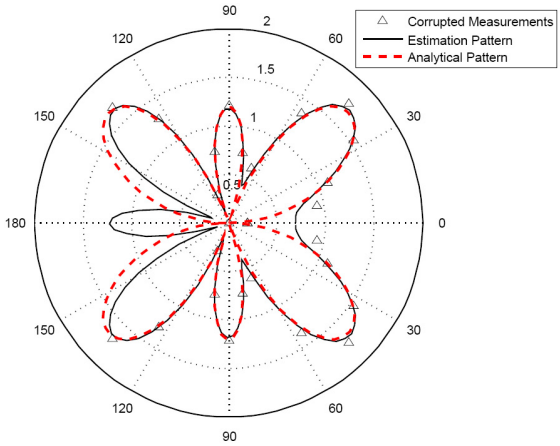

Fig. 8. Radiation pattern estimation for a $3\lambda/2$ dipole with corrupted data with spherical harmonic decomposition up to $N = 8$. The observations are given for $0 \leq \theta \leq 140°$ and $0 \leq \phi \leq 360°$.

measurements based on the priori knowledge that the signal spherical harmonic expansion is finite dimensional. The algorithm can be regarded as projections involving two subspaces, the modelimited subspace and the space selection subspace, corresponding to the modelimited signal and given measurements. The iterative algorithm reduces the mean-square error between the spherical harmonic coefficients of the estimated and that of the original signal at successive iterations. Thus, the estimates tend to the original function over the whole sphere. A practical example of antenna radiation pattern reconstruction with corrupted data is given.

References

[1] R.B. Blackman and J.W. Tukey, *The Measurement of Power Spectra*, New York: Dover, 1958.

[2] D. Slepian, H.O. Pollak, and H.J. Landau, "Prolate spheroidal wave functions, Fourier analysis and uncertainty," *Bell Syst. Tech. Jounal*, vol. 40, no. 1, pp. 43–84, 1961.

[3] A. Papoulis, "A new algorithm in spectral analysis and band-limited extrapolation," *IEEE Trans. Circuits and Syst.*, vol. CAS-22, no. 9, pp. 735–742, Sept. 1975.

[4] D.A. Hayner and W.K. Jenkins, "The missing cone problem in computer tomography," *Advances in Computer Vision and Image Processing*, vol. 1, pp. 83–144, 1984.

[5] E.W. Hobson, *The Theory of Spherical and Ellipsoidal Harmonics*, New York: Chelsea, 1955.

[6] J.R. Driscoll and D.M. Healy, "Computing Fourier transforms and convolutions on the 2-sphere," *Advances in Applied Mathematics*, vol. 15, pp. 202–250, 1994.

[7] K. Atkinson, "Numerical integration on the sphere," *J. Aust. Math. Soc. B. Appl. Math.*, vol. 23, pp. 332–347, 1982.

[8] A.V. Oppenheim, R.W. Schafer, and J.R. Buck, *Discrete-Time Signal Processing*, Prentice Hall: Upper Saddle Rive, NJ, 2nd edition, 1999.

[9] E.G. Williams, *Fourier Acoustics: Sound Radiation and Nearfield Acoustical Holography*, Academic Press, 1999.

[10] R.J. Allard and D.H. Werner, "The model-based parameter estimation of antenna radiation patterns using windowed interpolation and spherical harmonics," *IEEE Trans. on Antennas and Propagation*, vol. 51, no. 8, pp. 1891–1906, August 2003.

[11] W.L. Stutzman and G.A. Thiele, *Antenna Theory and Design*, New York: Wiley, 1981.